Article

An atomistic thermodynamics study of the structural evolution of the Pt₃Ni(111) surface in an oxygen environment

SUN Dapeng, ZHAO Yonghui, SU Haiyan, LI Weixue *

State Key Laboratory of Catalysis, Dalian Institute of Chemical Physics, Chinese Academy of Sciences, Dalian 116023, Liaoning, China

ARTICLE INFO

ABSTRACT

The structural evolution of the Pt₃Ni(111) surface under oxidizing conditions was studied by ab initio atomistic thermodynamics. The thermodynamic phase diagram from Ni-rich to Pt-rich conditions with oxygen coverages up to one monolayer was constructed from their 560 possible surface structures. With an increase in the oxygen chemical potential, there were only two types of thermodynamically stable structures, which were a clean Pt-skin surface and a Ni-skin surface with chemisorbed oxygen, regardless of the underlying Pt-rich or Ni-rich conditions. Bimetallic surfaces with chemisorbed oxygen were only metastable. The detail analysis revealed that the structural evolution is determined by the factors of segregation cost, difference between oxygen-metal (Pt and Ni) bonding strength, and oxygen chemical potential.

1. Introduction

Alloys, especially bimetallic alloy systems comprising Pt and a non-noble transition metal (TM), are widely used as catalysts [1–10] because they have unique activities in various catalytic reactions, such as water-gas-shift reaction [11], oxygen reduction reaction [12–15], and hydrogenation [16,17]. The Pt-Ni alloy has received special attention because it was found that the Pt₃Ni(111) surface with a Pt-skin surface exhibited a much higher activity for oxygen reduction that was ten times that of Pt(111) and 90 times higher than a commercialized Pt/C catalyst [18]. Also, a "sandwich-like" structure comprising NiO₁₋ₓ/ Pt/Ni/Pt(111) has shown the highest activity for CO oxidation [19]. It was further found that the surface structures of the Pt-Ni bimetallic system changed reversibly under the different conditions of an oxidizing or a reducing atmosphere [20,21].

These results indicated that the chemical properties of an alloy surface such as its reactivity, selectivity, and stability strongly depend on its composition, structure, and chemical state. Under a reactive environment, the adsorption of reactants on the alloy surface can result in surface reconstruction, segregation, and oxidation or reduction, which affect the catalytic mechanism and activity [22]. A systematic and quantitative study of the structural evolution of the alloy surface under a catalytic reaction environment can reveal the important factors that should be considered in the design and improvement of the stability and activity of the catalyst.

This work is a comprehensive study of surface segregation and oxidation under an oxygen environment of the Pt₃Ni(111) surface by an ab initio atomistic thermodynamic method [23–25]. We discuss the role of the bulk alloy reservoir by considering the effect of a small amount of non-stoichiometry in a Pt₃Ni bulk alloy. The thermodynamic surface phase diagram of Pt₃Ni(111) under an oxygen environment was constructed. In addition, we analyzed the influence of the segregation energy, difference in the oxygen binding energy to Pt and Ni, and the

oxygen chemical potential on the structural evolution.

2. Methods

2.1. Gibbs free energy of formation of the alloy surface under an oxygen environment

For a given temperature T and oxygen partial pressure p_{O2}, the stability of the alloy surface is described by the Gibbs free energy of formation, which is defined as follows for the Pt-Ni bimetallic system:

$$\gamma = (G_s - N_s x_{Pt} \mu_{Pt} - N_s x_{Ni} \mu_{Ni} - N_O \mu_O)/A \quad (1)$$

where N_s and N_O are the numbers of metal atoms and oxygen atoms in the system, and x_{Pt} and x_{Ni} are the mole factions of Pt and Ni ($x_{Pt} + x_{Ni} = 1$). A is the normalized surface area, which is equal to the twice of one side surface area of the center-symmetric model as below. G_s is the Gibbs free energy of the alloy system, which is usually approximately equal to the total energy E_s [24]. μ_O is the oxygen chemical potential at a specified temperature and pressure condition:

$$\mu_O = 0.5 \times (E_{O2} + \Delta\mu_{O2}(T, p°) + k_B T \ln(p_{O2}/p°)) =$$
$$0.5 \times E_{O2} + \Delta\mu_O(T, p_{O2}) \quad (2)$$

where k_B is the Boltzmann constant, and E_{O2} is the total energy of an isolated O_2 molecule. $\Delta\mu_{O2}(T, p°)$ can be obtained from tabulated enthalpy and entropy values at the standard pressure $p° = 0.1$ MPa. μ_{Pt} and μ_{Ni} are the chemical potentials of Pt and Ni, respectively. For bulk Pt₃Ni alloy in equilibrium, $4\mu_{Pt3Ni} = 3\mu_{Pt} + \mu_{Ni}$, where μ_{Pt3Ni} is the chemical potential of the Pt₃Ni alloy, which is approximately equal to the total energy per atom (E_{Pt3Ni}) of the bulk Pt₃Ni alloy. Eq. (1) can be rewritten as

$$\gamma \approx (E_s - N_s E_{Pt3Ni} - N_s \Delta\mu_{Pt\text{-}Ni}(x_{Pt} - 0.75) - 0.5 \times$$
$$N_O E_{O2} - N_O \Delta\mu_O(T, p_{O2}))/A \quad (3)$$

where $\Delta\mu_{Pt\text{-}Ni} = \mu_{Pt} - \mu_{Ni}$ is the difference between the chemical potentials of Pt and Ni in the alloy system, and 0.75 is the mole faction of Pt in stoichiometric bulk Pt₃Ni.

With a Pt-rich or Ni-rich condition, the corresponding chemical potential μ_{Pt} or μ_{Ni} in the alloy is higher. However, their values are lower than that of pure bulk Pt or Ni, namely, $\mu_{Pt} \leq \mu_{Pt(fcc)}$ and $\mu_{Ni} \leq \mu_{Ni(fcc)}$, because otherwise the Pt-Ni alloy will not be stable. Because $4\mu_{Pt3Ni} = 3\mu_{Pt} + \mu_{Ni}$, $\Delta\mu_{Pt\text{-}Ni}$ can only vary in range

$$\Delta\mu_{Pt\text{-}Ni} \text{ (Ni-rich)} \leq \Delta\mu_{Pt\text{-}Ni} \leq \Delta\mu_{Pt\text{-}Ni} \text{ (Pt-rich)} \quad (4)$$

where $\Delta\mu_{Pt\text{-}Ni}$ (Ni-rich) $= (\mu_{Pt3Ni} - \mu_{Ni(fcc)})/0.75$, and $\Delta\mu_{Pt\text{-}Ni}$ (Pt-rich) $= 4(\mu_{Pt(fcc)} - \mu_{Pt3Ni})$. By approximating $\mu_{Pt(fcc)}$ and $\mu_{Ni(fcc)}$ by the total energy of bulk face centered cubic (fcc) Pt and Ni, $E_{Pt(fcc)}$ and $E_{Ni(fcc)}$, the lower and upper limits of $\Delta\mu_{Pt\text{-}Ni}$ are $\Delta\mu_{Pt\text{-}Ni}$ (Ni-rich) $= -0.67$ eV and $\Delta\mu_{Pt\text{-}Ni}$ (Pt-rich) $= -0.32$ eV, respectively.

Equation (3) indicates that the Gibbs free energy of formation of the alloy surface depends on the relative contents of Pt and Ni, and also on the chemical potential of oxygen. We note that under a high $\Delta\mu_O$, the alloy surface can be oxidized to surface oxides and even bulk oxides. For simplicity, we limit the present work to the chemisorption regime with oxygen coverages up to one monolayer (ML) only. These results from oxygen chemisorption as a precursor, however, provide valuable insights for the subsequent oxidation.

2.2. Computational details

Spin-polarized density functional theory (DFT) calculations were performed using the Vienna Ab initio Simulation Package (VASP) [26,27] using the all-electron projected augmented wave (PAW) potentials [28,29] and the Perdew-Wang 91 (PW91) exchange-correlation functional [30]. The wave function was expanded in plane waves with a kinetic cutoff of 400 eV. The Monkhorst-Pack method (containing the Γ point) was used for k-point sampling in the reduced Brillouin zone. For the bulk fcc structures of Pt, Ni, and Pt₃Ni, a grid of (12×12×12) was used. The optimized lattice constants were a_0(Pt) = 0.399 nm, a_0(Ni) = 0.352 nm, and a_0(Pt₃Ni) = 0.389 nm, which agreed well with a previous study [31]. The alloy surfaces were simulated by using the (1×1) structures of center-symmetric slab models with 7 layers, and the two identical surfaces were separated by a vacuum of 1.5 nm. The middle 3 layers were fixed as the bulk while the other layers were fully relaxed during structure optimization. For the oxygen covered surfaces, oxygen atoms were allowed to adsorb symmetrically on both sides of the unit cell. (6×6×1) Monkhorst-Pack k-point grids were used in the surface structure calculations. For the computation of gaseous oxygen, a (1.45 nm × 1.50 nm × 1.56 nm) cell was used. The force convergence for all structural relaxation was set to less than 0.1 eV/nm.

3. Results and discussion

The structure of the bulk Pt₃Ni alloy is L1₂, with a stoichiometric ratio of 3:1 for Pt:Ni in the bulk. For the Pt₃Ni(111)-(1×1) surface, each layer contains three Pt atoms and one Ni atom. In order to study the effect of nonstoichiometry, the ratios of Pt:Ni in the outer two layers (for each side of the symmetric cell) were allowed to change gradually from 8:0 (Pt-rich condition) to 0:8 (Ni-rich condition), while the bulk phase (the middle 3 layers) was fixed at 3:1. Taking into account the relative positions of the bulk atoms, there are 35 possible substrate configurations. Based on these clean surface structures, oxygen adsorption was considered by placing from zero up to four O atoms on each side of the unit cell onto the fcc sites, which corresponded to oxygen coverages θ_O = 0.00, 0.25, 0.50, 0.75, 1.00 ML, respectively. A combination of $C_4^0 + C_4^1 + C_4^2 + C_4^3 + C_4^4 = 16$ possible O adsorption configurations for the surface grid was obtained (θ_O = 0 ML was considered one type of adsorption). From these, we constructed 560 (35×16) possible structures. They were some equivalent surface structures, but to make it easier to manipulate in the batch program, we kept all the configurations. We calculated the total energy of each configuration after structure optimization by DFT and used this in Eq. (3) to get the relative stability of the configurations for different oxygen chemical potentials under Ni-rich (Fig. 1) and Pt-rich (Fig. 2) conditions. A higher coverage of oxygen gave a steeper slope of the lines of Gibbs free energy of formation, and a higher sensitivity to the oxygen environment. For a given oxygen chemical potential, the surface configuration with the lowest Gibbs free energy of formation (the lowest line in Fig. 1 and Fig. 2) is the thermodynamically most favorable structure.

3.1. The phase diagram of the Pt₃Ni(111) surface

Figure 1 shows the Gibbs free energy of formation of the Pt₃Ni(111) surface under Ni-rich conditions versus the oxygen chemical potential $\Delta\mu_O$. At the very low oxygen chemical potential conditions of $\Delta\mu_O < -1.68$ eV that pertain to a high temperature and low pressure (see the upper axes of Fig. 1), the most stable surface structure is a clean Pt-skin structure with 100% Pt in the first layer and 100% Ni in the second layer. As illustrated in Fig. 1(a), the outer two layers have a Pt-Ni ratio of 4:4, which is lower than the bulk value (3:1), manifesting a Ni-rich condition. With increasing oxygen chemical potential, the dissociative adsorption of oxygen on the surface becomes exothermic, and the coverage of oxygen increases gradually. When $\Delta\mu_O > -1.68$ eV, a structure of $\theta_O = 0.50$ ML with 100% Ni in the first layer (Ni-skin) and Pt:Ni = 3:1 in the second layer is the most stable (Fig. 1(b)). In this structure, the Pt-Ni ratio in the outer two layers is 3:5, which is also a Ni-rich condition. Under the condition of $\Delta\mu_O > -1.58$ eV, the most stable structure is shown in Fig. 1(c), with an oxygen coverage of $\theta_O = 0.75$ ML. At even higher oxygen chemical potentials of $\Delta\mu_O > -0.62$ eV, the coverage of oxygen reaches 1 ML, as shown in Fig. 1(d). During the evolution of the surface from Fig. 1(b) to 1(d), the configurations in the outer two layers are the same as in Fig. 1(b), and the Pt-Ni ratio is always 3:5 under the Ni-rich condition.
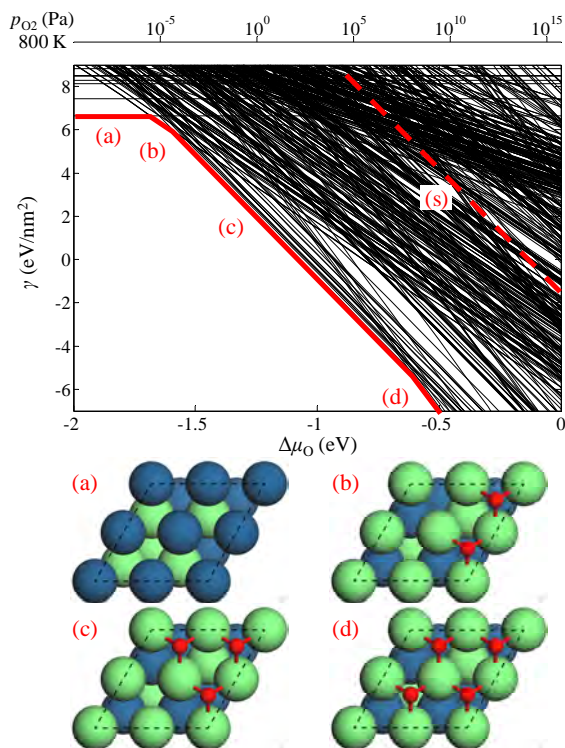
It should be emphasized that we considered all possible compositions and configurations with different oxygen coverages. With increasing oxygen chemical potential, there are only two types of stable structures, namely, the clean Pt-skin surface and the Ni-skin surfaces with $\theta_O \geq 0.50$ ML. There were no Pt-Ni bimetallic surfaces (e.g. the stoichiometric Pt₃Ni surface in Fig. 1(s), with the schematic structure shown in Fig. 2(s)) nor structures with oxygen coverages less than 0.25 ML that exists as stable structures, that is, these are only metastable. The reason is the interplay between the segregation energies and oxygen-metal binding energies of Pt and Ni, which will be discussed later.

The phase diagram of Pt₃Ni(111) under a Pt-rich condition is presented in Fig. 2. When $\Delta\mu_O < -1.48$ eV, the most stable surface is composed of 100% Pt in the first layer (Pt-skin) and Pt:Ni = 3:1 in the second layer without any adsorbed O on the surface (Fig. 2(a)). With increasing oxygen chemical potential, the dissociative adsorption of oxygen on the surface starts to be exothermic, and the coverage of oxygen increases correspondingly. Our calculations show that when $\Delta\mu_O > -1.48$ eV, a structure of $\theta_O = 0.75$ ML with 100% Ni in the first layer (Ni-skin) and 100% Pt in the second layer is the most stable (Fig. 2(b)). At the even higher oxygen chemical potentials of $\Delta\mu_O > -0.68$ eV, the coverage of oxygen reaches 1 ML, as shown in Fig. 2(c), where the configurations in the outer two layers of this Ni-skin surface are the same as Fig. 2(b).

Similarly to the Ni-rich condition, with increasing oxygen chemical potential, there are only two types of stable surface structures, namely, the Pt-skin surface without adsorbed O and the Ni-skin surfaces with $\theta_O \geq 0.50$ ML. Pt-Ni bimetallic surfaces (e.g. the stoichiometric Pt₃Ni surface alloy in Fig. 2(s)) and

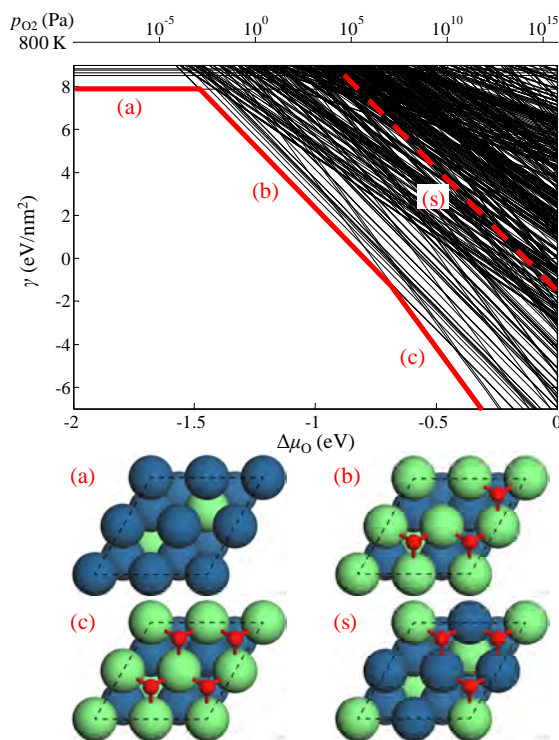**Fig. 1.** Surface free energy of Pt₃Ni(111) versus oxygen chemical potential $\Delta\mu_O$ under Ni-rich condition. Each line corresponds to one possible surface configuration. The red segments (a, b, c, and d) represent the most stable structure for the range of $\Delta\mu_O$. The corresponding structures (top view) are shown at the bottom. The red dashed line (s) corresponds to the stoichiometric Pt₃Ni(111) surface with $\theta_O = 0.75$ ML, as shown in Fig. 2(s). The blue, green, and red balls are, respectively, Pt, Ni, and O atoms. The correlation between $\Delta\mu_O$ and oxygen partial pressure at 800 K is indicated at the top.

Fig. 2. Surface free energy of Pt₃Ni(111) versus oxygen chemical potential $\Delta\mu_O$ under a Pt-rich condition.

structures with oxygen coverage of 0.25, and 0.50 ML are only metastable.

3.2. Segregation energy and oxygen-metal binding

To understand the above results, we define three quantities as follows:

$$E_{seg} = E_s^{clean} - E_{s(Pt3Ni)}^{clean} - N_s\Delta\mu_{Pt-Ni}(x_{Pt} - 0.75) \quad (5)$$
$$E_b = (E_s - E_s^{clean} - 0.5 \times N_O E_{O2})/N_O \quad (6)$$
$$\gamma_{Pt3Ni} = (E_{s(Pt3Ni)}^{clean} - N_s E_{Pt3Ni})/A \quad (7)$$

where E_{seg} is the segregation energy, which is the energy cost of the particular surface configuration (without adsorbates) with respect to the stoichiometric surface, and E_s^{clean} and $E_{s(Pt3Ni)}^{clean}$ are the corresponding total energies. E_b is the average adsorption energy per O atom on the particular surface. γ_{Pt3Ni} is the surface energy of the stoichiometric Pt$_3$Ni(111) surface. Equation (3) can be rewritten as

$$\gamma \approx \gamma_{Pt3Ni} + (E_{seg} + N_O E_b - N_O\Delta\mu_O(T, p_{O2}))/A \quad (8)$$

Equation (8) indicates that the Gibbs free energy of formation of a particular surface is determined by the segregation energy E_{seg}, average O adsorption energy E_b, and oxygen chemical potential in addition to the surface energy of stoichiometric Pt$_3$Ni(111). The dependence of E_{seg} and E_b on composition and configuration will be discussed below.

We first calculated E_{seg} for all the structures considered. Figure 3 is the calculated E_{seg} (per unit surface area) as a function of the Pt concentration in the topmost layer (x_{Pt}). At a given x_{Pt}, only the result with the least segregation energy is plotted. Regardless of the structures present under Pt-rich or Ni-rich conditions, the segregation energies decrease linearly with x_{Pt}. When x_{Pt} is more than 75%, E_{seg} even becomes negative (exothermic). This implies that in the absence of oxygen adsorption, Pt atoms tend to segregate to the surface. This is understandable because the surface energy of Pt(111) is lower than that of Ni(111) [32]. As seen in Fig. 3, when the surface configuration changes from the Ni-skin ($x_{Pt} = 0\%$, containing 4 Ni atoms in the top layer of the unit surface area) to the Pt-skin ($x_{Pt} = 100\%$, containing 4 Pt atoms in the top layer of the unit surface area), the segregation energy decreases by 2.54 (Pt-rich) and 1.97 (Ni-rich) eV. That is, there is an average energy cost of 0.56 eV/atom when a surface Pt atom is substituted by a bulk Ni
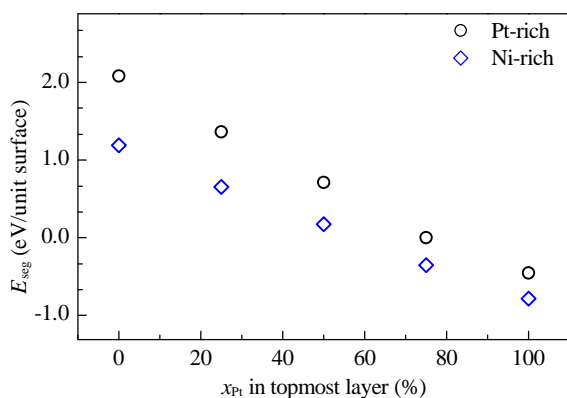

Fig. 4. Average adsorption energy of oxygen as a function of the percentage of O–Pt bonds over all O–metal bonds, $x_{O-Pt} = N(O-Pt)/(N(O-Pt) + N(O-Ni))$, for different coverages of oxygen. The line is a linear interpolation between the average adsorption energy of oxygen (0.25 ML) on Ni(111) and Pt(111) surfaces and is given as a guide to the eye.

atom.

Using Eq. (6), we calculated the average oxygen dissociative adsorption energy (E_b) and studied its dependence on surface composition and oxygen coverage. For a given oxygen coverage, the calculated E_b was very sensitive to the percentage of O–Pt bonds of all the O–metal bonds (x_{O-Pt}). As shown in Fig. 4, E_b increases with x_{O-Pt}. This means that the oxygen-metal bond strength decreases with more O–Pt bond, which is understandable because the O–Ni bond strength is higher than that of the O–Pt bond, as seen from the calculated oxygen average adsorption energy of –2.44 and –1.23 eV on Ni(111) and Pt(111) at $\theta_O = 0.25$ ML. It was found further that at a given x_{O-Pt}, a higher coverage of oxygen gave a higher average adsorption energy, which was due to the increase of lateral repulsion between adsorbed oxygen. From the above results, the difference in the O–metal bond strength between O–Ni and O–Pt on Pt$_3$Ni and their dependence on oxygen coverage were extracted. For $\theta_O = 0.25$ ML, when x_{O-Pt} increases from 0% (three O–Ni bonds) to 100% (three O–Pt bonds), E_b decreases by 1.62 eV. Thus an O–Ni bond strength is on average 0.54 eV stronger than that of the O–Pt bond. With the increase of oxygen coverage to 0.50, 0.75, and 1.00 ML, the difference in the bond strength increases to 0.64, 0.69, and 0.70 eV, respectively.

3.3. The trends of oxygen-induced segregation

The above analysis indicates that once a Ni atom segregates onto the surface by substituting for a Pt atom, the energy of the system rises about 0.56 eV. As a consequence, at a low oxygen chemical potential without dissociative oxygen adsorption, the segregation of the more noble metal is preferred in order to minimize the total Gibbs free energy, which finally gives a clean Pt-skin surface. While increasing oxygen chemical potential in the range of $\Delta\mu_O > -1.68$ eV (Ni-rich, Fig. 1) or $\Delta\mu_O > -1.48$ eV (Pt-rich, Fig. 2), oxygen from the gas environment starts to adsorb dissociatively on the surface. From Fig. 4, we note that when $\theta_O = 0.25$ ML, the difference between the O–Ni bond strength and O–Pt bond strength is 0.54 eV, which would not compensate for the cost of the segregation energy of Ni atom

Fig. 3. Segregation energy per (1×1) surface as a function of Pt concentration in the topmost layer (x_{Pt}) for all the clean surface configurations. Only the lowest value at each x_{Pt} is shown.
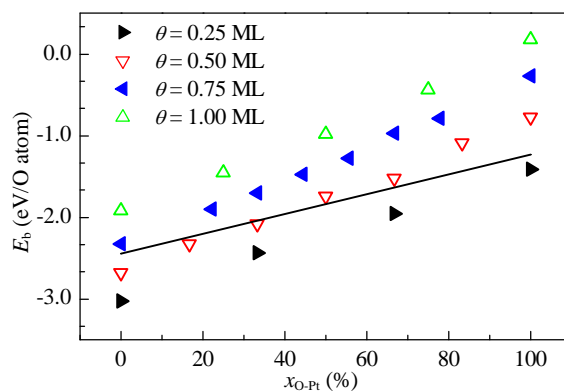
from the bulk to the surface (about 0.56 eV). However, when θ_O ≥ 0.50 ML, the difference between the O–Ni bond strength and O–Pt bond strength increases to 0.64, 0.69, and 0.70 eV respectively, which are all large enough to compensate the cost of the segregation energy. On the other hand, when θ_O ≥ 0.50 ML, all metals on the top layer will bind to at least one O atom.

Thus, once the thermodynamic condition for oxygen dissociative adsorption is reached, oxygen-induced Ni segregation will occur to maximize the O–Ni bonds, so that a Ni-skin surface with θ_O ≥ 0.50 ML chemisorbed O will be formed, if there is no kinetic restrictions. To better see why the Pt-Ni bimetallic surfaces are only metastable, we consider a stoichiometric Pt₃Ni(111) surface with a oxygen coverage of 0.75 ML. Although its segregation energy is lower than that of the Ni-skin surface, the weaker O–Pt bond leads to a higher Gibbs free energy of formation (shown by the red dashed lines (s) in Figs. 1 and 2) compared to the Ni-skin surface with the same oxygen coverage.

For oxygen-induced segregation to cause the change from the Pt-skin to Ni-skin, the corresponding oxygen chemical potential should be $\Delta\mu_O$ = −1.68 eV (Ni-rich) and $\Delta\mu_O$ = −1.48 eV (Pt-rich). As indicated in the top panel of Figs. 1 and 2, these correspond to oxygen partial pressures of 3.5×10^{-6} Pa (Ni-rich) and 1.2×10^{-3} Pa (Pt-rich) at 800 K, respectively. At 300 K, they are equivalent to 5.6×10^{-43} Pa (Ni-rich) and 2.9×10^{-36} Pa (Pt-rich), which are far less than possible at ultra-high vacuum (UHV) conditions. This means that oxygen-induced Ni segregation to form the Ni-skin surface occurs easily at elevated temperatures. However, with possible kinetic hindrance at low temperatures, metastable structures can however be formed.

There is no systematic experimental study of Pt₃Ni(111) under oxidizing conditions so far. However, there was an experimental study of the Pt(111) surface deposited with 1.3 ML Ni [21]. It was found that at UHV and 800 K (corresponding to $\Delta\mu_O$ < −1.8 eV), all the Ni atoms diffused into the subsurface region to leave a Pt-skin surface. On increasing the pressure to

p_{O2} = 5.2×10^{-5} Pa ($\Delta\mu_O$ = −1.6 eV), most Ni atoms segregated onto the surface and a NiO film was formed. Considering the errors in the DFT calculations from the exchange-correlation functional and the difference between the Pt₃Ni(111) alloy and the 1.3 ML Ni/Pt(111) system, the agreement between theory and experiment is satisfactory. The experimental study also found that when the temperature was decreased to 700 K but with the same oxygen pressure of p_{O2} = 5.2×10^{-5} Pa, there was less Ni segregation and oxidation. Because the corresponding oxygen chemical potential (equivalent to $\Delta\mu_O$ = −1.4 eV) was even higher than that at the higher temperature, this means that kinetic hindrance to Ni segregation on Pt₃Ni(111) was present at 700 K.

4. Conclusions

A systematic ab initio atomistic thermodynamics study on the structural evolution of the Pt₃Ni(111) surface with oxygen adsorption up to 1 ML coverage was performed. With increasing oxygen chemical potential, there are only two types of thermodynamically stable structures, namely, the clean Pt-skin surface and Ni-skin surfaces with oxygen coverage higher than 0.50 ML. The interplay between the segregation energy and the difference in oxygen bonding strength between Pt and Ni plays an essential role in the structural evolution in the presence of oxygen. Surface alloys are metastable, but they can be formed when there is kinetic hindrance to structural change.
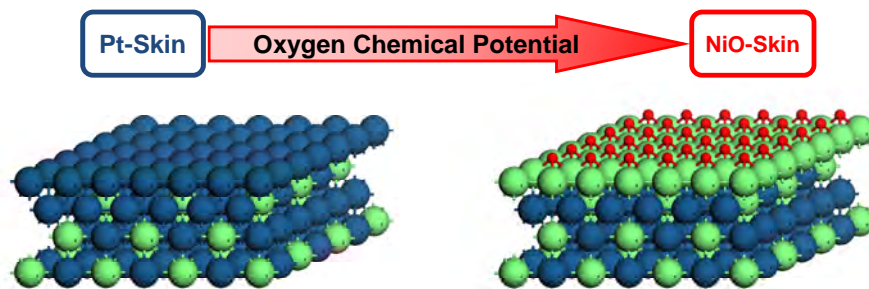
References

[1] Shao Y Y, Yin G P, Gao Y Z. *J Power Sources*, 2007, 171: 558
[2] Ferrando R, Jellinek J, Johnston R L. *Chem Rev*, 2008, 108: 845
[3] Antolini E, Lopes T, Gonzalez E R. *J Alloys Compd*, 2008, 461: 253
[4] Peng Z M, Yang H. *Nano Today*, 2009, 4: 143
[5] Wang D S, Li Y D. *Adv Mater*, 2011, 23: 1044
[6] Fu Q, Li W X, Yao Y X, Liu H Y, Su H Y, Ma D, Gu X K, Chen L M, Wang Z, Zhang H, Wang B, Bao X H. *Science*, 2010, 328: 1141

An atomistic thermodynamics study of the structural evolution of the Pt₃Ni(111) surface in an oxygen environment

SUN Dapeng, ZHAO Yonghui, SU Haiyan, LI Weixue*
Dalian Institute of Chemical Physics, Chinese Academy of Sciences

With a gradual increase of oxygen chemical potential, the clean Pt-skin surfaces of Pt₃Ni(111) transit to the oxygen-chemisorbed Ni-skin surfaces without stable oxygen-chemisorbed PtNi surface alloys formed.

[7] Sun D P, Gu X K, Ouyang R H, Su H Y, Fu Q, Bao X H, Li W X. *J Phys Chem C*, 2012, 116: 7491

[8] Su H Y, Bao X H, Li W X. *J Chem Phys*, 2008, 128: 194707

[9] Ma X F, Deng H Q, Yang M M, Li W X. *J Chem Phys*, 2008, 129: 244711

[10] Ma X F, Su H Y, Deng H Q, Li W X. *Catal Today*, 2011, 160: 228

[11] Knudsen J, Nilekar A U, Vang R T, Schnadt J, Kunkes E L, Dumesic J A, Mavrikakis M, Besenbacher F. *J Am Chem Soc*, 2007, 129: 6485

[12] Marković N M, Ross P N Jr. *Surf Sci Rep*, 2002, 45: 117

[13] Stamenkovic V, Mun B S, Mayrhofer K J J, Ross P N, Markovic N M, Rossmeisl J, Greeley J, Norskov J K. *Angew Chem, Int Ed*, 2006, 45: 2897

[14] Greeley J, Jaramillo T F, Bonde J, Chorkendorff I, Norskov J K. *Nat Mater*, 2006, 5: 909

[15] Chen S, Ferreira P J, Sheng W C, Yabuuchi N, Allard L F, Shao-Horn Y. *J Am Chem Soc*, 2008, 130: 13818

[16] Skoplyak O, Menning C A, Barteau M A, Chen J G. *Top Catal*, 2008, 51: 49

[17] Chen J G, Menning C A, Zellner M B. *Surf Sci Rep*, 2008, 63: 201

[18] Stamenkovic V R, Fowler B, Mun B S, Wang G, Ross P N, Lucas C A, Markovic N M. *Science*, 2007, 315: 493

[19] Mu R T, Fu Q, Xu H, Zhang H, Huang Y Y, Jiang Z, Zhang S, Tan D L, Bao X H. *J Am Chem Soc*, 2011, 133: 1978

[20] Mu R T, Fu Q, Liu H Y, Tan D L, Zhai R S, Bao X H. *Appl Surf Sci*, 2009, 255: 7296

[21] Mu R T, Guo X G, Fu Q, Bao X H. *J Phys Chem C*, 2011, 115: 20590

[22] Zafeiratos S, Piccinin S, Teschner D. *Catal Sci Technol*, 2012, 2: 1787

[23] Kitchin J R, Reuter K, Scheffler M. *Phys Rev B*, 2008, 77: 075437

[24] Reuter K, Scheffler M. *Phys Rev B*, 2003, 68: 045407

[25] Li W-X, Stampfl C, Scheffler M. *Phys Rev Lett*, 2003, 90: 256102

[26] Kresse G, Hafner J. *Phys Rev B*, 1993, 48: 13115

[27] Kresse G, Furthmuller J. *Phys Rev B*, 1996, 54: 11169

[28] Bloechl P E. *Phys Rev B*, 1994, 50: 17953

[29] Kresse G, Joubert D. *Phys Rev B*, 1999, 59: 1758

[30] Perdew J P, Chevary J A, Vosko S H, Jackson K A, Pederson M R, Singh D J, Fiolhais C. *Phys Rev B*, 1992, 46: 6671

[31] Ma Y, Balbuena P B. *Surf Sci*, 2008, 602: 107

[32] Su H Y, Gu X K, Ma X F, Zhao Y H, Bao X H, Li W X. *Catal Today*, 2011, 165: 89

氧气气氛下Pt₃Ni(111)表面结构变化的从头算原子热力学研究

孙大鹏，赵永慧，苏海燕，李微雪*

中国科学院大连化学物理研究所催化基础国家重点实验室, 辽宁大连116023

摘要: 采用从头算原子热力学方法系统研究了Ni-rich和Pt-rich条件下Pt₃Ni(111)在不同偏析、表面化学吸附氧覆盖度下560个可能结构的相对稳定性, 构建了氧气气氛下Pt₃Ni(111)表面结构演化、直至满覆盖化学吸附氧的热力学相图. 结果表明, 随着氧的化学势的升高, 在热力学上仅出现两类稳定的结构, 主要包括没有化学吸附氧的干净Pt-skin表面, 以及在很低氧的化学势下就形成的含有化学吸附氧的Ni-skin表面, 而有化学吸附氧的PtNi表面合金化的中间结构则处于亚稳态. 仔细分析发现, 这些结构的形成主要由金属的偏析能、氧与两种金属成键强弱的差别、氧的化学势的高低三个因素共同决定.

关键词: Pt₃Ni; 氧气; 偏析; 相图; 从头算

1. 前言

合金催化剂广泛应用于多相催化反应中, 近年来尤以Pt基贵金属与活泼金属形成的二元合金体系的研究居多[1~10]. 在水煤气变换[11]、氧还原[12~15]和加氢反应[16,17]中, 合金表面因其双功能特点而往往成为催化反应的活性中心. 作为燃料电池工业的一种电极催化剂, Pt-Ni合金因具有比纯Pt更高的活性和更强的抗CO中毒能力, 而引起广泛的关注. 研究发现, Pt₃Ni(111)表面对氧还原催化活性比Pt(111)表面提高了一个数量级, 而比工业中使用的Pt/C催化剂提高了近两个数量级[18]. 通过调变Pt-Ni体系的制备条件以及切换氧化或还原气氛, 能够可逆地改变表面结构, 发现通过控制温度和反应气氛得到的"三明治"结构NiO₁₋ₓ/Pt/Ni/Pt(111), 相比Pt-Ni体系其它结构, 显示出最高的CO氧化反应活性[19~21].

综上可见, 合金催化剂的活性、选择性及稳定性与其表面的组分、化学价态和结构紧密相关. 合金表面的几何结构和电子结构等性质既不同于各单独组分, 又不同于合金的体相. 在实际反应气氛下, 反应物分子在合金表面吸附或解离, 由于分子与合金的各组分间的相互作用存在差异, 导致合金表面的化学组分和化学价态发生变化, 从而直接影响催化剂的机理和性能[22]. 因此, 系统定量地研究制备条件和真实反应条件下Pt-Ni合金表面组分结构的变化规律, 并揭示其内在的作用机制, 对于正确揭示反应机理、优化催化剂的设计、提高性能和稳定性具有重要的意义.

基于从头算的原子热力学方法[23~25], 本文系统研究了在不同氧气气氛下Pt₃Ni(111)面的结构演化, 并考虑

到合成Pt_3Ni合金过程中Pt和Ni含量可能的变化, 定量地研究了该合金表面偏析和表面氧化的行为, 从而构造了表面化学吸附氧直至一个单层时的热力学相图; 此外, 从偏析能、吸附能和氧气化学势等因素出发, 揭示氧化诱导表面偏析的热力学本质及其相互制约的关系, 以期对类似体系的制备和反应条件下结构稳定性的研究有所启发.

2. 理论研究方法

2.1. 氧气气氛下合金表面热力学

在任意给定的温度T和氧气压力p_{O2}情况下, 合金表面的稳定性由其表面形成自由能来描述, 相应的自由能越低, 表面越稳定. 以Pt-Ni双金属合金为例, 其表面形成自由能为:

$$\gamma = (G_s - N_s x_{Pt} \mu_{Pt} - N_s x_{Ni} \mu_{Ni} - N_O \mu_O)/A \quad (1)$$

其中, N_s和N_O分别是体系金属原子和氧原子的总数; x_{Pt}和x_{Ni}分别是体系中Pt和Ni的摩尔分数, 且$x_{Pt} + x_{Ni} = 1$; A为表面面积, 在下文所述中心对称的单胞模型下, 是一侧表面单胞面积的2倍; G_s是扩展体系的吉布斯自由能, 通常情况下可近似为体系总能E_s[24]. 给定温度和压力下氧的化学势μ_O为:

$$\mu_O = 0.5 \times (E_{O2} + \Delta\mu_{O2}(T, p°) + k_B T \ln(p_{O2}/p°)) = \\ 0.5 \times E_{O2} + \Delta\mu_O(T, p_{O2}) \quad (2)$$

其中k_B为波尔兹曼常数, E_{O2}为孤立氧分子的总能, $\Delta\mu_{O2}(T, p°)$可在热力学手册中查得($p° = 0.1$ MPa). μ_{Pt}和μ_{Ni}分别是Pt和Ni的化学势. 对于本文所研究的Pt_3Ni有序体相合金, 在热力学平衡时$4\mu_{Pt3Ni} = 3\mu_{Pt} + \mu_{Ni}$, 其中$\mu_{Pt3Ni}$是$Pt_3Ni$体相合金的化学势, 可近似为$Pt_3Ni$体相合金每个原子的平均总能$E_{Pt3Ni}$. 考虑到实际的材料合成过程中所用Pt和Ni源不同, 使得相应的化学势有所变化, 所生成的合金中Pt和Ni的含量会与理论计量比发生一定的偏差, 进而影响合金在氧气气氛下的结构演化. 为了很好地描述这一情况, 将方程(1)改写为:

$$\gamma \approx (E_s - N_s E_{Pt3Ni} - N_s \Delta\mu_{Pt-Ni}(x_{Pt} - 0.75) - 0.5 \times \\ N_O E_{O2} - N_O \Delta\mu_O(T, p_{O2}))/A \quad (3)$$

其中, $\Delta\mu_{Pt-Ni} = \mu_{Pt} - \mu_{Ni}$. 为了保证$Pt_3Ni$合金相的稳定而不发生两相分离, Pt和Ni的化学势不能任意变化, 必须满足$\mu_{Pt} \leq \mu_{Pt(fcc)}$和$\mu_{Ni} \leq \mu_{Ni(fcc)}$. 其中$\mu_{Pt(fcc)}$和$\mu_{Ni(fcc)}$分别是体相fcc Pt和fcc Ni的化学势, 分别对应于富铂(Pt-rich)和富镍(Ni-rich)的极端情况. 根据$4\mu_{Pt3Ni} = 3\mu_{Pt} + \mu_{Ni}$, 可以推导出$\Delta\mu_{Pt-Ni}$允许变化的范围:

$$\Delta\mu_{Pt-Ni}(\text{Ni-rich}) \leq \Delta\mu_{Pt-Ni} \leq \Delta\mu_{Pt-Ni}(\text{Pt-rich}) \quad (4)$$

其中, $\Delta\mu_{Pt-Ni}$ (Ni-rich) = $(\mu_{Pt3Ni} - \mu_{Ni(fcc)})/0.75$, $\Delta\mu_{Pt-Ni}$ (Pt-rich) = $4(\mu_{Pt(fcc)} - \mu_{Pt3Ni})$. 以体相fcc Pt和fcc Ni的总能$E_{Pt(fcc)}$和$E_{Ni(fcc)}$近似$\mu_{Pt(fcc)}$和$\mu_{Ni(fcc)}$, 可算得$\Delta\mu_{Pt-Ni}$的边界条件为$-0.67$ eV (Ni-rich)和-0.32 eV (Pt-rich).

由式(3)可见, 表面形成自由能不仅与Pt和Ni的含量有关, 还取决于氧的化学势. 在较高的氧的化学势下, 合金表面可能会生成表面氧化物, 并最终完全氧化形成稳定的体相氧化物, 从而出现两相分离. 本文主要研究合金表面氧化的情况, 即表面化学吸附氧的覆盖度仅达到1个单层(1 ML)时的结构, 而有关深度氧化的研究不在此列.

2.2. 模型选择和计算方法

自旋极化总能计算和结构优化采用基于密度泛函理论(DFT)和周期性模型的VASP程序包[26,27], 原子赝势采用PAW势[28,29], 使用广义梯度近似(GGA)的PW91泛函[30], 平面波截断能为400 eV. 用包含Γ点的Monkhorst-Pack格点方法对k空间简约Brillouin区分布取点, 对于体相fcc结构Pt, Ni, 以及Pt_3Ni, k点选取(12×12×12). 优化的晶格常数分别为$a_0(Pt) = 0.399$ nm, $a_0(Ni) = 0.352$ nm和$a_0(Pt_3Ni) = 0.389$ nm, 与文献[31]一致. 合金表面采用7层(1×1)中心对称的原子超晶胞模型, 中间三层固定为体相结构, 其余部分完全弛豫, 所有的氧吸附构型同样保持中心对称, 真空层厚度为1.5 nm, k点选取(6×6×1). E_{O2}的计算采用(1.45 nm × 1.50 nm × 1.56 nm)的正交晶胞. 所有结构优化的力收敛条件为小于0.1 eV/nm.

3. 结果与讨论

体相Pt_3Ni合金的晶体结构为$L1_2$, Pt-Ni化学计量比为3:1. $Pt_3Ni(111)$-(1×1)晶胞内每层包括3个Pt原子和1个Ni原子. 为了研究在Pt-rich和Ni-rich两种情况下Pt和Ni含量的变化, 本文考察了表面两层共计8个金属原子相对含量发生变化的情况, 相应的Pt:Ni比例从8:0逐渐变化到0:8, 而体相(中间三层) Pt:Ni仍然维持在3:1. 考虑到相对位置的变化, 共得到35个不等价的表面结构. 对于氧原子的解离化学吸附, 为简单起见, 我们仅考察了氧原子在稳定的fcc位吸附, 且吸附氧原子的个数从0逐渐增至4, 即对应于氧覆盖度$\theta_O = 0.00, 0.25, 0.50, 0.75, 1.00$ ML. 在不考虑吸附衬底构型影响下, 共有$C_4^0 + C_4^1 + C_4^2 + C_4^3 + C_4^4 = 16$种吸附构型, 从而共得到560种可能表面构型. 由这些不同的构型计算所得的总能, 带入到方程(3)中, 即可得到Ni-rich (见图1)和Pt-rich (见图2)情况下各种可能的结构在不同氧化学势下的相对稳定性. 在

相同的氧化学势下, 氧原子的覆盖度越大, 相应结构的表面形成自由能斜率越大, 对气氛的变化也越敏感, 而表面形成自由能最低的结构对应于热力学上最稳定的结构.

3.1. Pt₃Ni(111)表面相图

Ni-rich条件下的表面相图见图1. 在氧的化学势极低条件下, $\Delta\mu_O < -1.68$ eV (对应于高温、低压的情况, 参见图1上与化学势相对应的温度和压力值), 最稳定的结构为表层全部由Pt原子组成而次表层全部为Ni原子组成的没有氧化学吸附的干净Pt-skin表面(见图1(a)). 此时, 表面两层的Pt-Ni的计量比为4:4, 低于相应的体相值(3:1), 即对应于Ni-rich的情况. 随着氧的化学势的升高, 氧开始在表面上发生解离吸附, 并且表面氧的覆盖度也逐渐变大. 当$\Delta\mu_O > -1.68$ eV时, 形成$\theta_O = 0.50$ ML表面暴露原子全部是Ni原子而次表层Pt:Ni = 3:1的稳定结构(见图1(b)). 此时, 表面两层所有金属原子的计量比为Pt:Ni = 3:5, 仍然是对应于Ni-rich的情况. 当$\Delta\mu_O > -1.58$ eV时, 表面氧的覆盖度达到$\theta_O = 0.75$ ML, 形成的稳定结构见图1(c). 当$\Delta\mu_O > -0.62$ eV时, $\theta_O = 1.00$ ML, 形成的结构见图1(d). 在这些结构变化过程中, 表面两层所有金属原子Pt:Ni计量比和构型与$\theta_O = 0.50$ ML的相同, 没有发生变化.

需要强调的是, 上述计算涵盖了在不同的Pt和Ni含量变化、相对位置以及氧覆盖度情况下所有可能形成的表面结构. 随着$\Delta\mu_O$的增加, 所得最稳定的表面结构中没有出现$\theta_O = 0.25$ ML的中间结构; 同时最稳定的表面结构表面组分从没有氧化学吸附的Pt-skin的结构直接过渡到Ni-skin的结构, 没有PtNi表面合金化的中间结构出现. 这是由于偏析能与氧-金属键能之间的差异和竞争所致, 具体原因将在下文讨论.

Pt-rich条件下的表面相图见图2. 当$\Delta\mu_O < -1.48$ eV时, 氧分子未在表面上发生解离吸附. 这时形成表面全部由Pt原子组成而次表层Pt:Ni = 3:1的最稳定的Pt-skin表面(见图2(a)). 随着氧化学势的升高, 氧开始在表面上发生解离吸附, 并且表面氧的覆盖度也逐渐增加. 当$\Delta\mu_O > -1.48$ eV时, 形成$\theta_O = 0.75$ ML, 此时表面暴露的全是Ni原子(Ni-skin), 而次表层全为Pt原子(见图2(b)). 当$\Delta\mu_O > -0.68$ eV时, Ni-skin表面上的氧覆盖度将会达到1 ML, 次表层仍然全是Pt原子(图2(c)).

同样地, 随着$\Delta\mu_O$由低到高变化, 所形成的表面最稳定的结构并未出现$\theta_O = 0.25$, 0.50 ML的中间结构; 与Ni-rich相同, 外表面的金属组分从没有氧化学吸附的

Pt-skin结构直接过渡到有氧化学吸附的Ni-skin结构, 并未出现稳定的有氧化学吸附的表面PtNi合金中间结构.

3.2. 吸附诱导表面偏析的贡献因素

为了理解上述计算结果, 揭示控制相应结构变化的物理本质, 定义了如下三个物理量:

$$E_{seg} = E_s^{clean} - E_{s(Pt3Ni)}^{clean} - N_s\Delta\mu_{Pt-Ni}(x_{Pt} - 0.75) \quad (5)$$

$$E_b = (E_s - E_s^{clean} - 0.5 \times N_O E_{O2})/N_O \quad (6)$$

$$\gamma_{Pt3Ni} = (E_{s(Pt3Ni)}^{clean} - N_s E_{Pt3Ni})/A \quad (7)$$

其中E_{seg}为偏析能, 对应于所考察的不同Pt和Ni含量时各种可能的合金表面与按照体相结构中断的理想Pt₃Ni(111)表面的能差; E_s^{clean}和$E_{s(Pt3Ni)}^{clean}$为相应表面的总能. E_b为在相应的合金表面上的解离吸附氧原子的平均吸附能, γ_{Pt3Ni}是理想Pt₃Ni(111)表面的表面能. 相应地, 方程(3)可改写为:

$$\gamma \approx \gamma_{Pt3Ni} + (E_{seg} + N_O E_b - N_O\Delta\mu_O(T, p_{O2}))/A \quad (8)$$

方程(8)表示不同Pt和Ni含量情况下合金表面的形成自由能, 由相应的表面上的氧的平均解离吸附能、偏析能和理想Pt₃Ni(111)表面的表面能共同决定, 并且显著地依赖于氧的化学势.

图3是根据方程(5)算得不同Pt和Ni含量时干净表面最稳定结构的偏析能与相应的x_{Pt}之间的关系. 结果显示, 无论是在Pt-rich或Ni-rich条件下, 随着x_{Pt}增加, 偏析能近似于线性减小; 当x_{Pt}大于75%时, 偏析能甚至变为负值. 这说明在没有氧吸附的情况下, Pt倾向于在表面偏析. 这是是由于Pt的原子半径较大, 表面能相对较低所致[32]. 还可以发现, 当表面由Ni-skin ($x_{Pt} = 0$%, 单位(1×1)表面上包含有四个Ni原子)变为Pt-skin ($x_{Pt} = 100$%, 单位(1×1)表面上包含四个Pt原子)时, 偏析能降低了2.54 eV (Pt-rich)和1.97 (Ni-rich) eV. 这意味着将一个表面Pt原子替换为一个Ni原子需平均耗能0.56 eV.

根据方程(6)计算得到氧原子在不同表面上的平均解离吸附能, 结果见图4. 可以看出, 在给定氧覆盖度时, 随着O−Pt键在所有的氧-金属键中百分比(x_{O-Pt})增加, 平均解离吸附能逐渐升高, 化学键强度逐渐削弱, 这是由于O−Ni键强于O−Pt键所致. 以Ni(111)和Pt(111)为例, $\theta_O = 0.25$ ML时氧的平均吸附能分别为−2.44 eV/O和−1.23 eV/O; 另一方面, 相同x_{O-Pt}时, 随着氧覆盖度的增加, 平均解离吸附能逐渐升高, 对应于氧−金属化学键的强度逐渐削弱. 这是由于表面上带负电的氧原子之间存在静电偶极排斥所致: 氧覆盖度越高, 静电排斥越强. 由图4可得到不同Pt和Ni含量时合金表面上O−Ni和O−Pt键强度差别的定量结果以及随着氧覆盖度的变化关系. 在θ_O

= 0.25 ML时, 当x_{O-Pt}的比例从0%增至100%, 即表面完全由O−Ni键变为O−Pt键时, 氧的解离平均吸附能减小了1.62 eV. 因为所考察的氧吸附在fcc位, 每一个氧原子和三个金属原子成键, 这意味着所考察的合金表面上平均每个O−Ni键比O−Pt键要强0.54 eV. 当θ_O = 0.50, 0.75, 1.00 ML时, 相应的每个O−Ni键要比O−Pt键强0.64, 0.69和0.70 eV. 换言之, 随着氧覆盖度增加, O−Ni键与O−Pt键能差越来越大.

3.3. 吸附诱导表面偏析的总体趋势

上述分析表明, 每个Ni原子偏析到表面上将导致体系总能升高约0.56 eV. 因此, 在氧的化学势比较低、不发生化学吸附时, 热力学上为达到自由能最低, Pt尽可能在表面上偏析, 从而形成Pt-skin结构. 由图1和2可知, 当分别在$\Delta\mu_O > -1.68$ eV (Ni-rich)和$\Delta\mu_O > -1.48$ eV (Pt-rich)时, 氧开始在Pt-skin表面上化学吸附. 由图4可知, 当θ_O = 0.50和0.75 ML时, 每一个O−Ni键至少比O−Pt键分别强0.64和0.69 eV, 均大于偏析一个Ni原子到表面上的偏析能(~0.56 eV). 同时, 当$\theta_O \geq 0.50$ ML时, 所有暴露在表面上的金属原子都将至少和一个氧原子成键. 换言之, 一旦氧可以在Pt-skin表面上发生解离吸附, 如果没有氧诱导偏析所引起的扩散动力学上可能的限制, 解离吸附的氧原子将会诱导Ni完全偏析到表面上, 直接形成稳定的$\theta_O \geq 0.50$ ML化学氧吸附的Ni-skin结构(见图1(b)和图2(b)).

随着氧化学势的增加, 从没有氧化学吸附的Pt-skin结构, 直接形成有氧化学吸附($\theta_O \geq 0.50$ ML)的Ni-skin结构, 而中间没有其它的稳定结构, 如PtNi表面合金的结构出现. 为了更好地理解这一点, 用红色虚线标出图1和2中理想中断的计量比Pt$_3$Ni(111)表面上有化学吸附0.75 ML氧的表面所对应结构(见图2(s))的结果. 该表面上同时暴露有Pt和Ni原子, 且比例为3:1. 很明显, 虽然该表面的偏析能为零, 在能量上较Ni-skin更为有利, 但是由于表面上出现大量的Pt原子, O−Pt成键较O−Ni成键相对较弱, 其相应的表面形成自由能远高于同样氧覆盖度条件下Ni-skin所对应的结构(见图1(c)和图2(b)).

综上, 从Pt-skin变化到Ni-skin结构的条件为$\Delta\mu_O = -1.68$ eV (Ni-rich)和$\Delta\mu_O = -1.48$ eV (Pt-rich). 如图1和2所示, 在800 K时, 相对应氧的压力为3.5×10^{-6} Pa和1.2×10^{-3} Pa. 当温度降低到300 K时, 由方程(2)算得所需氧压降为5.6×10^{-43} Pa和2.9×10^{-36} Pa (已超出当前实验所能达到的真空条件); 此时尽管所需氧的压力非常低, 但是较低的温度导致结构变化可能会受到扩散动力学的限制, 并不一定出现热力学上最稳定的结构, 相反可能只生成一些亚稳态的中间结构.

迄今为止, 尚未见有关氧化气氛下Pt$_3$Ni结构变化的系统研究, 但Pt(111)单晶上沉积Ni (= 1.3 ML)的实验发现[21], 在800 K超高真空条件下($\Delta\mu_O < -1.8$ eV), 沉积的Ni全部扩散至次表层, 形成Pt-skin结构; 而当$p_{O_2} = 5.2 \times 10^{-5}$ Pa时($\Delta\mu_O = -1.6$ eV), 大部分Ni被偏析出表面形成NiO薄膜. 考虑到理论计算交换关联泛函近似以及本文计算对象的不同, 可以认为理论和实验结果较为一致. 实验还发现, 当温度降至700 K时, 维持氧压不变, 尽管此时氧的化学势($\Delta\mu_O = -1.4$ eV)更高, Ni可被氧化得更为彻底, 但实验发现, 被氧化诱导偏析出来的Ni含量有所降低. 这说明在700 K时, Ni由次表层偏析扩散到表面上来已经开始受动力学上限制. 值得注意的是, 当表面氧达到满覆盖度并进一步形成NiO膜时, 氧气的活化和扩散动力学的受限将变得较为显著, 从而现象有效抑制合金表面的深度氧化.

4. 结论

采用从头算原子热力学方法和大量的理论计算系统研究了氧化气氛下Pt$_3$Ni(111)表面化学吸附氧直至满覆盖度情况下的热力学相图. 研究发现, 随着氧化学势的升高, 在热力学上仅出现没有氧化学吸附的干净Pt-skin表面和有氧化学吸附的Ni-skin表面两种特征结构, 而没有形成PtNi表面合金的中间结构. 这主要是由于O−Ni键与O−Pt键强度差刚好能够补偿Ni和Pt的偏析能差. 另外, 当氧的化学势较低时, 合金表面倾向于从干净的Pt-skin表面转变为有化学吸附氧的Ni-skin表面. 形成较低的氧从Pt-skin表面由不同的Pt、Ni源(Ni-rich和Pt-rich)所制备的Pt$_3$Ni合金在氧化气氛下结构演化差别不大. 该研究主要集中在热力学上, 而未考虑动力学限制以及表面深度氧化; 而在实际条件下, 可能达不到热力学平衡, 因此也可能出现含有氧化学吸附的、PtNi表面合金的亚稳态中间结构; 而表面氧化膜的形成和钝化则可能会在动力学上抑制合金表面的深度氧化. 本文所采用的理论和分析方法具有一般性, 对于研究Pt$_3$Ni(111)双金属催化剂在实际氧化条件下的活性相结构及反应机理具有重要的参考价值.